Biophysical Journal Volume 109 December 2015 2307–2316

Article

Evaluating the Raftophilicity of Rhodopsin Photoreceptor in a Patterned Model Membrane

Yasushi Tanimoto,[1] Keisuke Okada,[1] Fumio Hayashi,[2,*] and Kenichi Morigaki[1,3,*]

[1]Graduate School of Agricultural Science, [2]Graduate School of Science, and [3]Research Center for Environmental Genomics, Kobe University, Kobe, Japan

ABSTRACT Lipid rafts in the cell membrane are believed to affect various membrane functions, including the signaling by G-protein coupled receptors (GPCRs). However, the regulatory roles of lipid rafts on GPCRs' functions are still poorly understood, partially owing to the lack of the methods to quantitatively evaluate the affinity of membrane proteins to lipid raft (raftophilicity). Here, we describe a methodology to gauge the raftophilicity of a representative GPCR in vertebrate photoreceptor, i.e., rhodopsin (Rh), and its cognate G protein transducin (G_t) by using a patterned model membrane. We generated a substrate-supported planar lipid bilayer that has patterned regions of liquid-ordered (L_o) and liquid-disordered (L_d) membrane domains. We reconstituted Rh and G_t into the patterned membrane and observed their lateral distribution and diffusion. Mobile and functional Rh molecules could be reconstituted through the rapid dilution of solubilized Rh, by optimizing the reconstitution conditions including the chamber design, protein/detergent concentrations, and solution mixing. We determined the partition and diffusion coefficients of Rh and G_t in the L_o-rich and L_d-rich regions. Both Rh and G_t were predominantly localized in the L_d phase, suggesting their low affinity to lipid rafts. Patterned model membrane offers a robust and scalable platform for systematically and quantitatively studying the functional roles of lipid rafts in biological membranes including retinal disk membranes.

INTRODUCTION

Heterogeneous distributions of lipids and proteins in the cell membrane are profoundly affecting the membrane functions. Lipid rafts enriched with saturated phospholipids, cholesterol, and some types of proteins are believed to regulate a wide range of cellular functions, including cell signaling and proliferation, and are associated with diseases such as cancer and diabetes (1–3). The functional roles of lipid rafts in the signal transduction of G protein-coupled receptors (GPCRs), the largest super family of human genome and the most important target of currently available drugs, are attaining heightened attention (4–6). The interactions between GPCR and rafts are reported to affect the dimer formation of GPCR and receptor signaling (7). However, the regulatory roles of lipid rafts on GPCRs' functions are still poorly understood, partially owing to the lack of the methodology to quantitatively evaluate the affinity of membrane proteins to lipid raft (raftophilicity).

The photoreceptor rhodopsin (Rh) is a GPCR that has been most extensively studied. Upon absorbing a photon, Rh undergoes conformational changes to metarhodopsin II (Rh*), which can activate the G protein transducin (G_t). Although Rh is thought to have a low affinity to lipid raft as the other intrinsic membrane proteins (2), Rh has tandem palmitoyl residues at the carboxyl terminus of eighth helix (8), so that it also has raftophilic singular point on its membrane spanning surface. G_t is a lipidated protein that attaches onto the surface of bilayer with hydrocarbon chains (9,10). Our previous biochemical study has shown that ~15% of Rh is in detergent-resistant membrane fractions (DRM) prepared from rod photoreceptor membranes (11). Furthermore, the affinity of G_t to the DRM was enhanced after photoirradiation in the rod outer segments (ROS), suggesting that the Rh*-G_t complex was associated with lipid rafts (11). These observations suggest that the raftophilicity of Rh is involved in an essential process of the G protein activation. More generally, a large number of studies indicate that the functions of Rh are strongly affected by the surrounding lipids (12,13). However, the roles of lipid rafts in regulating the signal transduction of Rh have not been fully understood. One important physical parameter for understanding the roles of lipid rafts is the raftophilicity. Although the association of molecules to DRM suggests their affinity to lipid raft (6,14), association to DRM itself is not suitable for quantitatively evaluating raftophilicity, because it is prone to artifacts during the solubilization and separation processes (15).

Artificial model membranes are potentially useful tools for quantitatively evaluating the physicochemical properties of membrane-bound molecules. Phase separation of liquid-ordered (L_o) and liquid-disordered (L_d) phases in giant unilamellar vesicles (GUVs) and giant plasma membrane

Submitted April 24, 2015, and accepted for publication October 8, 2015.

*Correspondence: fhayashi@port.kobe-u.ac.jp or morigaki@port.kobe-u.ac.jp

Editor: Andreas Engel.

0006-3495/15/12/2307/10

http://dx.doi.org/10.1016/j.bpj.2015.10.015

vesicles (GPMVs) has been extensively studied for mimicking lipid rafts. Partitioning of membrane-bound molecules in L_o/L_d phases has been used as a measure of raftophilicity (16–18). Another class of model membrane that has been used for studying membrane domains is substrate-supported planar lipid bilayer (SPB), which typically consists of a single lipid bilayer adsorbed on a hydrophilic substrate surface (e.g., glass). The L_o/L_d partitioning of urokinase receptors and integrin has been evaluated in SPBs (19,20). Micropatterning techniques can also be applied to SPBs for generating a patterned array of L_o and L_d domains (21,22). SPBs with spatially well-defined membrane domains should provide a robust and scalable platform for systematically and quantitatively studying the raftophilicity of a wide variety of membrane proteins.

Here, we describe a methodology to gauge the raftophilicity of Rh and its cognate G protein (G_t) by using a patterned model membrane. We have previously developed an SPB that can spatially separate L_o/L_d domains by using a composite membrane of polymeric and fluid lipid bilayers (23). A patterned polymeric bilayer was lithographically generated from a diacetylene phospholipid by ultraviolet (UV) irradiation. The density of polymeric bilayer domains could be locally modulated by applying varied UV doses and removing nonreacted monomers with a detergent solution (Fig. 1 *A*) (24). As a fluid bilayer containing a mixture of saturated lipid, unsaturated lipid, and cholesterol was incorporated, L_o domains enriched with saturated lipid and cholesterol were concentrated in the polymer-free region (R_0), whereas L_d domains enriched with unsaturated lipid were accumulated in the partially polymeric region (R_1) (Fig. 1 *C*). Recently, we established a method to quantitatively control the spatial distribution of L_o and L_d domains (25). In this study, we reconstituted Rh and G_t from bullfrog (*Rana catesbeiana*) into the patterned SPB and observed their lateral diffusion and partitioning in R_0 and R_1 (Fig. 1 *D*). Reconstitution of GPCR into SPB generally poses significant technological challenges, although there have been some reports of successful reconstitution into tethered bilayers (12,26,27). We succeeded in reconstituting Rh in a fully mobile and functional state. We determined the partition and diffusion coefficients of Rh and G_t in the L_o-rich and L_d-rich membranes by the single molecule observation. The observations represent an important step toward quantitative understanding of the roles of lipid rafts in sorting proteins and modulating their interactions, in not only phototransduction but also general G protein signaling systems.

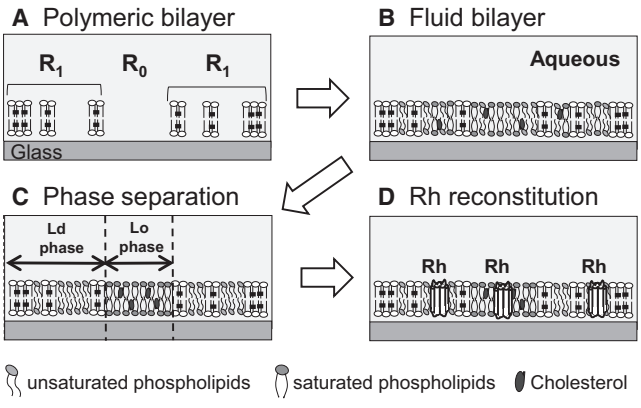

FIGURE 1 Schematic illustration of the patterned phase separation in a model membrane and incorporation of Rh. (*A*) The patterned membrane has two regions: polymer-free region (R_0) and partially polymeric region (R_1). (*B* and *C*) The fluid bilayer between polymeric bilayers spontaneously separate into L_o and L_d phases and accumulate in R_0 and R_1, respectively. (*D*) Rh is reconstituted into the SPB by the rapid dilution of detergent-solubilized Rh molecules.

MATERIALS AND METHODS

Materials

DiynePC (1,2-bis(10,12-tricosadiynoyl)-*sn*-glycero-3-phosphocholine), DOPC (1,2-dioleoyl-*sn*-glycero-3-phosphocholine), DPPC (1,2-dipalmitoyl-*sn*-glycero-3-phosphocholine), Chol (cholesterol (ovine wool)), and Rho-PE (1,2-dioleoyl-*sn*-glycero-3-phosphoethanolamine-N-lissamine rhodamine B) were purchased from Avanti Polar Lipids (Alabaster, AL). HiLyte Fluor 750 C2 maleimide (HL750) was from Anaspec (Fremont, CA), and Cy7-NHS-ester was from GE Healthcare (Piscataway, NJ). TR-PE (Texas Red 1,2-dihexadecanoyl-*sn*-glycero-phosphoethanolamine) was purchased from Molecular Probes (Eugene, OR). SDS (sodium dodecyl sulfate), OG (1-O-*n*-octyl-β-D-glucopyranoside), glucose oxidase, catalase, and glucose were purchased from Nacalai Tesque (Kyoto, Japan). BSA (bovine serum albumin) was purchased from Sigma-Aldrich (St. Louis, MO). Deionized water used in the experiments was ultrapure Milli-Q water (Millipore, Billerica, MA) with a resistance of 18.2 MΩ cm. It was used for cleaning substrates and preparing buffer solutions.

Purification of Rh and G_t

All procedures were done in complete darkness using infrared goggles (Nocto vision NVR-2015; NEC, Tokyo, Japan). ROS were prepared from retinas of bullfrogs (*Rana catesbeiana*) as described previously in Hayashi and Yamazaki (28). Rh was purified from ROS as described previously in Litman (29). Briefly, ROS membranes were washed with a hypotonic buffer (5 mM Tris-HCl, 5 mM dithiothreitol, pH7.5), and solubilized with 50 mM OG in buffer A (20 mM HEPES, 1 mM $MgCl_2$, 120 mM NaCl, pH7.5), and Rh was purified by Con A-Sepharose column (Amersham Pharmacia Biotech, Uppsala, Sweden). Approximately 4 mg/mL of Rh was obtained in buffer A containing 30 mM OG. The α- and $\beta\gamma$-subunit of G_t, i.e., $G\alpha_t$ and $G\beta\gamma_t$, were purified from frog ROS as described previously in Yamazaki et al. (30). The concentration of active Rh molecules was evaluated from the visible light absorption at 500 nm (31).

Protein labeling

Fluorescence-labeling of Rh was done as follows under infrared illumination. ROS containing 50 nmole Rh was washed with 1 mL of buffer B (10 mM MOPS, 60 mM KCl, 30 mM NaCl, 5 mM $MgCl_2$, 5 mM dithiothreitol, 5 μg/mL aprotinin, 2 μg/mL *n*-[*n*-(L-3-Trans-carboxirane-2-carbonyl)-L-leucyl]-agmatine (E-64), 2 μg/ mL leupeptin, pH 7.5) by ultracentrifugation (452,000 *g*, 5 min at 4°C) three times. ROS suspension in buffer B was mixed with Cy7-NHS dissolved in dimethyl sulfoxide (Rh/Cy7-NHS = 1:20). Reaction was proceeded for 2 min at 0°C, and stopped by adding 10 μmole of glycine. Cy7-labeled ROS were washed with buffer

A by ultracentrifugation three times as described above, and resulting pellet was solubilized with 0.1 mL of 100 mM OG in buffer A. After ultracentrifugation (65,000 *g*, 60 min at 4°C), supernatant was applied to Con A-Sepharose column (0.5 mL) equilibrated with buffer A containing 30 mM OG. Cy7-labeled Rh (Cy7-Rh) was eluted with 250 mM methyl α-D-mannoside in buffer A containing 30 mM OG. The column chromatography was done at room temperature in the darkness. The peak fraction contained 11.4 μM of Rh, and the dye/Rh ratio was 0.134.

To probe single Rh molecules, we used Fab′ fragment of monoclonal antibody IgG (1D4) against the C-terminal peptide of rhodopsin (RHO 1D4 from The University of British Columbia through Flintbox) (32). The Fab′ preparation and labeling with the SH-reactive dye were performed as described previously in Ichinose et al. (33). The Fab′ was labeled with HL750 and purified by Superose 12-3.2 × 300 (GE Healthcare) on Smart System (Amersham Pharmacia Biotech). Peak fraction of Fab′ was pooled and stored at −30°C as 50% glycerol-stock. The molar ratio of dye/Fab′ was estimated spectrophotometrically to be ~1 using the molar extinction coefficients (ε) 75,000 M^{-1} cm^{-1} at 280 nm for Fab′, and 250,000 M^{-1} cm^{-1} for HiLyte Fluor 750 (Anaspec). Complex of Rh and Fab′ (Rh-Fab′) was prepared by mixing nonlabeled Rh in the solubilized state and labeled Fab′ at the 1:1 molar ratio. We incubated the sample long enough (overnight at 4°C) to ensure stoichiometric formation of Rh-Fab′.

$G\alpha_t$ was directly labeled with HL750 and purified by the authentic methods as follows (34). Briefly, G_t molecules in light-bleached ROS (300 nmole of rhodopsin) were labeled with HL750 at 0°C for 40 min by adding an aqueous solution of HL750 (1.2 μmole). Labeled $G\alpha_t$ was extracted from the ROS membranes by the activation of $G\alpha_t$ with GTP. The extract was applied to a Blue-Sepharose column (1 mL in column volume), and bound HL750-$G\alpha_t$ was eluted with NaCl gradient (0–1 M). The peak fractions were pooled and concentrated by ultrafiltration (Amicon Ultra, 0.5 mL, 30 k), and stored at −30°C as 50% glycerol stock solution. Molar ratio of dye/$G\alpha_t$ was estimated to be ~0.7 using ε = 30,400 M^{-1} cm^{-1} at 280 nm for $G\alpha_t$, and 250,000 M^{-1} cm^{-1} for HiLyte Fluor 750 (Anaspec).

Substrate cleaning

Microscopy coverslips (Matsunami, Osaka, Japan) were used as substrates for bilayer deposition. The substrates were sonicated in an sodium dodecyl sulfate solution (0.1 M) for 20 min, rinsed with Milli-Q water (Millipore), treated in a solution of NH_4OH (28%)/H_2O_2 (30%)/H_2O (0.05:1:5) for 10 min at 65°C, rinsed extensively with Milli-Q water, and then dried in a vacuum oven for 30 min at 80°C. Before use, the substrates were further cleaned by the UV/ozone treatment for 20 min (PL16-110; Sen Lights, Toyonaka, Japan).

Preparation of patterned polymeric bilayer

Bilayers of monomeric DiynePC were deposited onto glass substrates by the spontaneous spreading of vesicles. DiynePC powder was suspended in Milli-Q water by freezing in liquid nitrogen and thawing at 60°C (five cycles). After the freeze-and-thaw, DiynePC suspension was homogenized by an ultrasonic homogenizer (Branson Sonifier 150, Branson Ultrasonics, Danbury, CT) at 60°C (30 s × 2). Monomeric DiynePC suspension was deposited onto a cleaned substrate on ice to immediately cool the membrane. (We previously discovered that it is important to deposit monomers at a low temperature for generating homogeneously polymerized DiynePC bilayers (35).)

Polymerization of DiynePC bilayers was conducted by UV irradiation using a mercury lamp (UVE-502SD; Ushio, Tokyo, Japan) as the light source. A closed system that comprised a water reservoir, a pump, and a chamber (~4 mL volume) was used. The water reservoir was depleted of oxygen by purging with argon, and oxygen-free water was continuously supplied to the chamber by the pump. The chamber had two walls on the opposite sides, one being the sample (the SPB was inside the chamber) and the other being a quartz window through which UV light was illuminated. Desired patterns were transferred to the SPB in the polymerization process by illuminating the sample through a photomask that was placed directly on the SPB. The surface coverage of polymeric bilayers was controlled by adjusting the applied UV dose. After sufficient circulation of deaerated water (typically 15 min), the pump was stopped and the polymerization was started. The applied UV intensity was typically 7 mW/cm^2 at 254 nm and the dose was varied by changing the illumination period. After the UV irradiation, nonpolymerized DiynePC molecules were removed from the substrate surface by immersing in 0.1 M SDS solution at 30°C for 30 min and rinsing with Milli-Q water extensively. The polymerized bilayers were stored in Milli-Q water in the dark at 4°C.

Preparation of vesicle suspensions

Three types of vesicle suspensions were prepared: 1) DOPC with TR-PE (1 mol %); 2) DOPC/DPPC/Chol (1:1:1) with G_{M1} and TR-PE (1% each); and 3) DOPC/DPPC/Chol (1:1:1) with G_{M1} and Rho-PE (1% each). DOPC, DPPC, Chol, and TR-PE (or Rho-PE) were dissolved in chloroform. G_{M1} was dissolved in methanol. Lipid solutions were mixed in a round-bottom flask, dried with nitrogen, and evaporated for 4 h in a vacuum desiccator. The dried lipid film was hydrated in PBS (phosphate-buffer saline, 0.01 M sodium phosphate buffer with 0.15 M NaCl, pH 7.0) (the total lipid concentration was 1 mM) overnight. Lipid membranes were dispersed by five freeze-and-thaw cycles, and the suspension was extruded by using a Liposofast extruder (Avestin, Ottawa, Canada) with 100 nm polycarbonate membrane filter (10 times) and 50 nm polycarbonate filter (15 times).

Phase separation in a patterned SPB

Patterned separation of L_o and L_d phases was induced in DOPC/DPPC/Chol (1:1:1) (with G_{M1} and TR-PE (or Rho-PE) (1% each)). A patterned polymeric bilayer containing polymer-free (R_0) and partially polymeric (R_1) regions was attached with a polydimethylsiloxane chamber for keeping the aqueous solution during the incubation and microscopic observation (see Fig. S1 in the Supporting Material). Subsequently, DOPC/DPPC/Chol vesicle suspension was introduced into the chamber and incubated overnight. (The vesicle fusion and phase separation occurred quickly, within 1 h, but we incubated much longer to complete the equilibration.) After the incubation, the vesicle suspension was rinsed with Milli-Q water (five times). If there were defects in the fluid bilayer (especially in R_0), we supplemented vesicle suspension into the chamber to fill the defects. After rinsing again with Milli-Q water, we filled the chamber with PBS buffer and the sample was observed by the fluorescence microscopy.

Reconstitution of Rh and G_t into the SPB

Rh was reconstituted into a preformed SPB by the rapid dilution of solubilized Rh molecules (12,27). Rh (either native, Cy7-labeled, or Fab′-bound) was diluted with 30 mM OG in PBS to the final concentration of 76 nM. A quantity of 10 μL of the diluted solution was quickly mixed with 400 μL of PBS in the chamber (the SPB was at the bottom of the chamber: see Fig. S1). For rapidly incorporating Rh into the bilayer, the solution was vigorously stirred with a magnet. Furthermore, vesicle suspensions of DOPC/DPPC/Chol were preadded to the PBS solution (total lipid concentration: 0.75 mM) to deplete excess Rh molecules. We repeated the introduction of Rh solution 10 times to increase the number of reconstituted Rh molecules. The final concentration of OG was 6 mM, and the Rh/lipid ratio was 2.53 × 10^{-5} (mol/mol). HL750-$G\alpha_t \cdot G\beta\gamma_t$ complex (HL750-G_t) was reconstituted into SPB by introducing a solution of HL750-G_t into the polydimethylsiloxane chamber, incubating for 1 min, and rinsing 5 times with buffer B.

Single molecule observation of Rh and G_t

Reconstituted Rh and G_t were observed by the total internal reflection fluorescence microscopy (TE2000-V; Nikon, Tokyo, Japan) equipped with a near infrared laser diode (SL750 nm 100T; Shanghai Sail Laser, Shanghai, China). Images were acquired by an electron-multiplying charge-coupled device camera (C9100-12; Hamamatsu Photonics, Hamamatsu, Japan) at 30 frames s^{-1} frame rate and 76 nm $pixel^{-1}$ spatial resolution. To minimize photobleaching during the observation, 2.5 μg/mL glucose oxidase, 2.5 μg/mL catalase, and 70 μg/mL glucose were added to the buffer solution.

Evaluation of the diffusion coefficients

The movement of single molecules was tracked by the TrackMate program in Fiji (ImageJ; National Institutes of Health, Bethesda, MD). Diffusion coefficients of Rh and G_t were evaluated by the mean-square displacement (MSD) analysis using a MATLAB (The MathWorks, Natick, MA) per-value class MSD analyzer (36). More than 100 trajectories with the minimum length of 15 and average length of ~30 were subjected to the MSD analyzer. The diffusion coefficients were calculated from the MSD-Δt plots of the trajectories using the equation

$$\left\langle r^2 \right\rangle = 4D_{100\mathrm{ms}}\Delta t^{\alpha}, \quad (1)$$

where $\langle r^2 \rangle$ is the MSD from origin (μm^2), $D_{100\mathrm{ms}}$ is the diffusion coefficient evaluated from the slope at 100 ms, and Δt is the time lag. The α is the anomalous coefficient, with $\alpha = 1$ value indicating Brownian diffusion and $\alpha \neq 1$ suggesting anomalous diffusion (37).

Evaluating the partition of Rh and G_t in the patterned SPB

We evaluated the partition of Rh and G_t in R_0 and R_1 as a measure of the raftophilicity. Molecules were counted in each image by the particle analysis program in ImageJ (National Institutes of Health). Only mobile molecules were counted by subtracting the average image from each individual image and deleting immobile particles. The densities of Rh and G_t were evaluated by dividing the numbers of counted molecules in R_0 and R_1 with the areas used for the analyses. The apparent partition coefficients (P_1) of Rh and G_t were determined as the ratio of molecular densities in R_1 and R_0:

$$P_1 = (d_1/d_0)/(1-p). \quad (2)$$

Here, p represents the area fraction of polymeric bilayer in R_1 and d_0 and d_1 are the density of counted molecules in R_0 and R_1, respectively. The number of molecules in R_1 was normalized with the area fraction of fluid bilayer (1–p), considering the fact that the region was partially occupied by polymeric bilayer. From the obtained apparent partition coefficients, we evaluated the L_d/L_o partition coefficients of Rh and Gt ($P_{Ld} = (d_{Ld}/d_{Lo})$: d_{Ld} and d_{Lo} are the calculated density of molecules in L_d and L_o, respectively) by using Rho-PE as a standard marker that partition completely in L_d phase (38). We evaluated the partition of Rho-PE in R_0 and R_1 from the ratio of fluorescence intensities in R_0 (I_0) and R_1 (I_1),

$$P_1^{\text{Rho-PE}} = (I_1/I_0)/(1-p). \quad (3)$$

The distribution of L_d and L_o phases in R_0 and R_1 were estimated from $P_1^{\text{Rho-PE}}$, according to our previous analysis (25):

$$a_1^{Ld} = P_1^{\text{Rho-PE}} a_0^{L_d}, \quad (4)$$

$$a_0^{Ld} = 0.5(1-A_1p)/\{(1-A_1)+A_1P_1^{\text{Rho-PE}}(1-p)\}. \quad (5)$$

Here, a_0^{Ld} and a_1^{Ld} are the area fractions of L_d phase in R_0 and R_1, respectively. The value A_1 represents the area fraction of R_1 in the patterned membrane (in this study, $A_1 = 0.75$). We assumed that the gross area fractions of L_o and L_d phases were 0.5 (equal area of the two phases) for the lipid composition used (DOPC/DPPC/Chol = 1:1:1). From the obtained values of P_1, $P_1^{\text{Rho-PE}}$, and a_0^{Ld}, we can obtain the L_d/L_o partition coefficient by using the following equation:

$$P_{Ld} = 1 + \frac{P_1 - 1}{a_0^{Ld}\left(P_1^{\text{Rho-PE}} - P_1\right)}. \quad (6)$$

Here, P_1 represents the apparent partition coefficient of either Rh or G_t.

RESULTS

Patterned phase separation

We prepared patterned membranes with locally modulated fractions of polymeric and fluid bilayer domains. Fig. 2 *A* shows the fluorescence micrographs of a patterned membrane comprising polymer-free region (R_0) and partially polymeric region (R_1). The circular regions of R_0 (4 μm in diameter) were surrounded by the grid-shaped R_1. R_1 contained both polymeric and fluid bilayers, whose area fractions could be varied by changing the applied UV dose for photopolymerization, as we previously demonstrated (24). The fluorescence intensity of the fluid bilayer in R_1 (I_1^{TR}) was lower than that in R_0 (I_0^{TR}) for a homogeneous bilayer

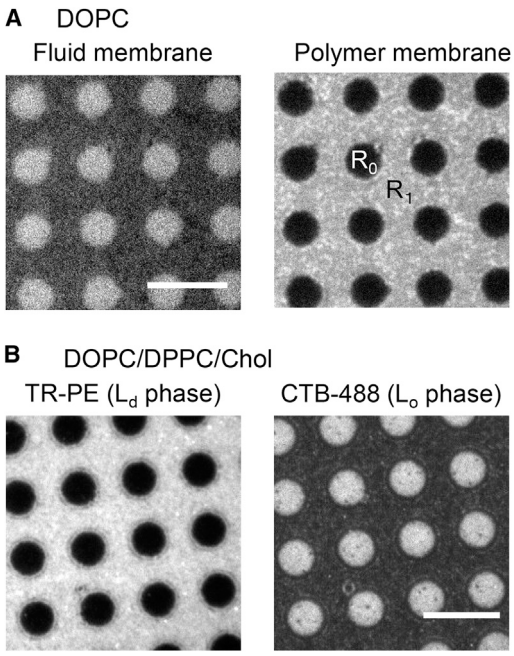

FIGURE 2 Fluorescence micrographs of the patterned phase separation: (*A*) a homogeneous bilayer (DOPC) was introduced. (*Left* and *right images*) Fluorescence from fluid bilayer (TR-PE) and polymeric bilayer (poly-diacetylene), respectively. The fluorescence of TR-PE in R_1 looked darker than R_0 due to the fact that R_1 is partially covered with polymeric bilayer. (*B*) The fluid bilayer was exchanged with a mixed lipid bilayer (DOPC/DPPC/Chol) and the phase separation was observed using the markers of L_d and L_o phases (TR-PE and CTB-488). The scale bar is 10 μm.

(DOPC/TR-PE), because R_1 was partially covered by polymeric bilayer (Fig. 2 *A*). The area fraction of polymeric bilayer in R_1 (p) was estimated from the fluorescence intensities by using the following equation (I_0^{TR} and I_1^{TR} represent the true fluorescence intensities after subtracting the background fluorescence intensity from the measured intensity):

$$p = 1 - \left(I_1^{TR}/I_0^{TR}\right). \quad (7)$$

For the sample in Fig. 2 *A*, p was estimated to be 0.26. After evaluating the p-values, we removed DOPC/TR-PE with a detergent solution (0.1 M SDS, 30 min at 30°C: this treatment did not alter polymeric bilayer domains) and incorporated a new lipid membrane (DOPC/DPPC/Chol (1:1:1) with TR-PE and G_{M1} (1 mol % each)) that separated into L_o and L_d phases. After incubation, TR-PE was enriched in R_1 (Fig. 2 *B*, *left*), as evidenced by the higher fluorescence intensity in R_1 compared with R_0, despite the fact that there was less fluid membrane in R_1 (note the inverted contrast between Fig. 2, *A* and *B*). To qualitatively detect the localization of L_o phase, we added CTB-488 after observing the distribution of TR-PE. CTB-488 was preferentially found in R_0 (Fig. 2 *B*, *right*).

Reconstitution of rhodopsin and transducin into the patterned membrane

Rh and G_t were reconstituted into the patterned bilayer after the phase separation. For the reconstitution of G_t, a solution of HL750-$G\alpha_t$ (0.7 μM) was mixed with $G\beta\gamma_t$ subunits (50 μM) to form a trimer (we call the fluorescently labeled trimer as HL750-G_t). HL750-G_t was added into the aqueous phase and we could observe the lateral diffusion of membrane-bound molecules (Fig. 3 and Movies S1 and S2). We generally did not observe any aggregation unless the incubation time was too long (>10 min). For reconstituting Rh, we needed a more elaborate procedure, because it is an integral membrane protein. We applied the approach to rapidly dilute solubilized Rh (12,27). Rh in the ROS membrane was fluorescently labeled with Cy7 (Cy7-Rh) or incubated with HL750-labeled Fab′ specific to the carboxyl terminus of Rh, and solubilized with OG with the final OG concentration of 30 mM. Reconstitution was conducted in a chamber comprising two layers of wells with different diameters (15 mm, *top layer* and 3.5 mm, *bottom layer*) (Fig. S1). The patterned membrane was in the bottom layer, whereas the top layer was designed to rapidly dilute Rh by mixing the solution with a magnetic stirring bar. The concentration of Rh was kept low to avoid aggregation during reconstitution. If we needed to reconstitute a higher concentration of Rh, we applied Rh solutions several times (up to 10 times). The maximum final concentration of Rh was 15.2 nM. On the other hand, the final concentration of OG was kept below its critical micellar concentration

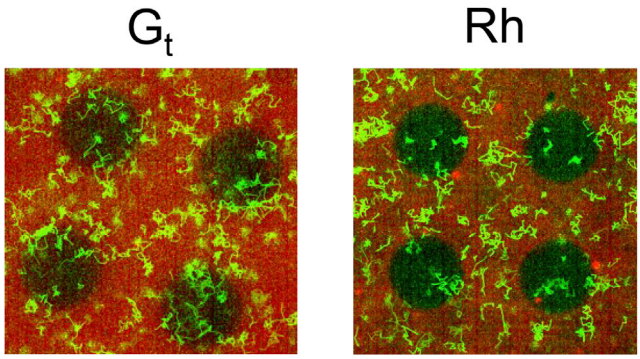

FIGURE 3 Single molecule observations of Rh and G_t: The trajectories of Cy7-Rh and HL750-G_t (100 frames) were overlaid with the fluorescence image of TR-PE in the patterned SPB. (*Grid-shaped regions*) R_1 enriched with the L_d phase; (*circular regions*) R_0 enriched with the L_o phase. The size of R_0 regions (corrals) was ~4 μm.

(25 mM) (39). To prevent the aggregation of Rh, we also initially added vesicle suspensions into the chamber (DOPC/DPPC/Chol: total lipid concentration = 0.75 mM). Vesicles served as a reservoir for the uptake of excess Rh. Vesicles also enabled to establish a defined ratio between Rh and lipid molecules. The maximum Rh/lipid ratio was 2.53×10^{-5} (mol/mol). By optimizing the reconstitution procedure, we could reconstitute Rh molecules in the mobile state (Fig. 3 and Movies S3 and S4). As we counted the number of mobile and immobile molecules, the fraction of mobile Rh ranged between 70 and 90% at the early stage of the observation. Due to photobleaching of fluorophore (Cy7), the number of mobile molecules decreased more quickly than that of immobile molecules during the observation. We suppose that the difference in photobleaching rate stems from the fact that immobile molecules consisted of aggregates. It should be noted that Rh were only partially labeled (the dye/Rh ratio was 0.134). Therefore, a large fraction of reconstituted Rh molecules were not observed. However, we believe that the presence of nonlabeled Rh did not influence the lateral mobility of Rh, because the diffusion coefficient was almost identical for Cy7-Rh and Rh-Fab′ (see below).

Diffusion coefficients of Rh and G_t were estimated by the MSD-Δt analysis of single molecule trajectories. Fig. 4 compares the diffusion coefficients of Cy7-Rh and Rh-Fab′ in the patterned membranes. From the trajectories of individual molecules ($N > 100$), the average MSD-Δt plots (Fig. 4 *A*) and the histogram of diffusion coefficients (Fig. 4 *B*) were obtained. The median diffusion coefficients were 0.28 $\mu m^2\ s^{-1}$ both for Cy7-Rh ($N = 119$) and Rh-Fab′ ($N = 142$). The fact that the diffusion coefficients were very close to each other suggested that the labeling method of Rh (direct conjugation of Cy7 or biding of HL750-Fab′) did not significantly alter the lateral diffusion of Rh molecules. To confirm that reconstituted Rh and G_t were functional, we reconstituted Rh (nonlabeled) and HL750-G_t into an SPB (DOPC/DPPC/Chol), and observed the changes of diffusion coefficients of HL750-G_t before and after the

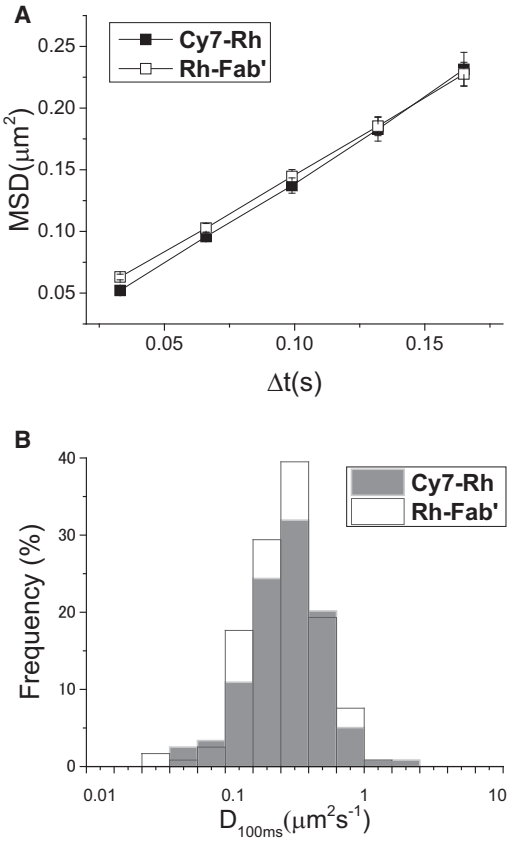

FIGURE 4 Diffusion coefficients of reconstituted Rh: Diffusion coefficients of two types of Rh (Cy7-Rh and Rh-Fab′) were obtained by the MSD versus time (Δt) plots. (*A*) The average MSD-Δt plots. (*B*) Histogram of the diffusion coefficients obtained from individual trajectories (Cy7-Rh: $N = 119$; Rh-Fab′: $N = 142$).

photoactivation of Rh and subsequent addition of GTP. Activated Rh (Rh*) and G_t should form tight complex and after GTP-GDP exchange would release GTP-$G\alpha_t$ from Rh* and $G\beta\gamma_t$ to allow free diffusion of GTP-$G\alpha_t$ (40). We observed that the diffusion of HL750-G_t decreased after the illumination from 0.60 $\mu m^2\ s^{-1}$ ($N = 118$) to 0.29 $\mu m^2\ s^{-1}$ ($N = 139$) (Fig. 5 *A*). As we added 500 μM GTP, the number of observed HL750-G_t significantly decreased and the diffusion was accelerated to 0.66 $\mu m^2\ s^{-1}$ ($N = 166$), indicating the dissociation of α-subunit (HL750-$G\alpha_t$) from the complex and membrane ((Fig. 5 *B*). On the other hand, addition of GTP in the dark condition (without activation of Rh) did not change the diffusion coefficient of HL750-G_t (the median diffusion coefficient was 0. 51 $\mu m^2\ s^{-1}$ ($N = 201$)) (Fig. 5 *C*). These results strongly support the premise that reconstituted Rh and G_t retained the functionality.

Localization of Rh and G_t in the patterned membrane

We analyzed the localization of Rh and G_t in the L_o-rich region (R_0) and the L_d-rich region (R_1) by counting the molecules in each region. Rh and G_t were predominantly observed in R_1, although individual molecules diffused freely between R_0 and R_1. The apparent partition coefficients between R_0 and R_1 ($P_1 = (d_1/d_0)/(1-p)$) were 1.42 ± 0.27 ($N = 11$) and 1.88 ± 0.43 ($N = 6$) for Cy7-Rh and HL750-G_t, respectively. From these values, we evaluated the partition coefficients in L_o and L_d phases by estimating the distribution of L_o and L_d domains in R_0 and R_1. Rho-PE was used as a marker of L_d domains (38). The distribution of L_o and L_d domains was determined from the fluorescence intensities of Rho-PE in R_0 and R_1. We determined the partition coefficient ($P_{Ld} = (d_{Ld}/d_{Lo})$) from the apparent partition coefficient and the distribution of L_d domains in R_0 and R_1. The average partition coefficients of Cy7-Rh and HL750-G_t were 5.19 ± 2.75 ($N = 11$) and 2.68 ± 0.69 ($N = 6$), respectively. Although the obtained values have rather large standard deviations, they clearly show that Rh and G_t have high affinities to L_d phase. It is important to note that P_{Ld} is not influenced by the amount of polymer in R_1 (p), whereas P_1 can be influenced by p because a higher degree of phase separation (localization of L_o and L_d domains) is induced by a larger amount of polymeric bilayer (25). To evaluate the possible effects of polymeric bilayer domains on the distribution of Rh, we reconstituted it into a patterned membrane containing a fluid bilayer from single lipid component (DOPC). The average image of 300 micrographs showed that more Rh molecules were observed in R_0 compared with R_1 (Fig. S2), reflecting the distribution of fluid bilayer (R_1 was partially covered with polymeric bilayer). This result suggests that Rh does not have any preference to R_0 or R_1 in the fluid bilayer. Furthermore, the partition coefficients obtained for individual samples did not show any significant dependency on the area fraction of polymeric bilayer (p) (Fig. S3). Therefore, we can exclude the possibility that polymeric bilayer domains are affecting the distribution of Rh and G_t.

The diffusion of individual molecules was analyzed separately in R_0 and R_1 by splitting the trajectories into the two regions. The diffusion coefficient of Cy7-Rh was estimated to be 0.23 $\mu m^2\ s^{-1}$ in R_0 ($N = 108$) and 0.36 $\mu m^2\ s^{-1}$ in R_1 ($N = 118$) (Fig. 6). On the other hand, the diffusion coefficient of HL750-G_t was estimated to be 0.67 $\mu m^2\ s^{-1}$ in R_0 ($N = 128$) and 0.24 $\mu m^2\ s^{-1}$ in R_1 ($N = 117$) (Fig. 6). The diffusion coefficient of Cy7-Rh was higher in R_1, whereas that of HL750-G_t was higher in R_0. It is expected that polymeric bilayer domains in R_1 should reduce the diffusion of both HL750-G_t and Cy7-Rh, depending on the amount of polymeric bilayer (p) (24). On the other hand, the retarded diffusion of Cy7-Rh in R_0 suggests that L_o domains containing a high content of DPPC and Chol decreased the lateral mobility of embedded Rh molecules. Because Rh is an integral membrane protein, its diffusion is expected to be more strongly influenced by the lipid membrane environment than G_t. We also estimated the anomalous diffusion of Rh and G_t from the MSD-Δt analysis by

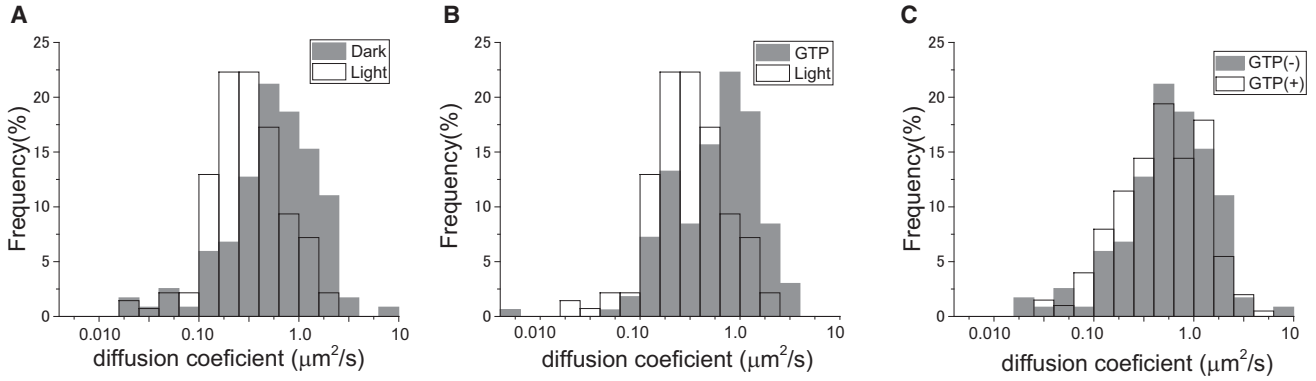

FIGURE 5 Evaluating the photoactivation of Rh: Rh (nonlabeled) and HL750-G_t were reconstituted into an SPB and the changes in diffusion coefficients of HL750-G_t were observed after light illumination (*A*), GTP addition (after light illumination (*B*), and in the dark state (*C*)). (*A*) $P < 0.01$; (*B*) $P < 0.01$; and (*C*) $P > 0.05$.

introducing the anomalous coefficient (α) (37). If $\alpha = 1$, molecules are diffusing randomly by the Brownian motion. On the other hand, if $\alpha \neq 1$ anomalous diffusion due to confinement or flow is implied. For Cy7-Rh, α was 0.89 ($N = 89$) in R_0 and 0.98 ($N = 116$) in R_1, respectively. For HL750-G_t, α was 0.97 ($N = 108$) in R_0 and 0.92 ($N = 109$) in R_1, respectively. These data suggest that both Rh and G_t were basically diffusing by the Brownian motion, although slight influences of confinement were observed for Cy7-Rh in R_0 and HL750-G_t in R_1.

DISCUSSION

We established a methodology to reconstitute Rh and G_t into a model membrane with micropatterned L_o and L_d phases. Mobile and functional Rh molecules could be reconstituted through the rapid dilution of solubilized Rh, by optimizing the conditions such as the chamber geometry, protein/detergent concentrations, and mixing conditions. Addition of vesicles to the solution was also critical for the successful reconstitution. It was observed that ~80% of Rh molecules (higher for G_t) were mobile in the patterned membrane. The observed diffusion coefficient of Rh shows fairly good agreement with those reported in a native membrane by classical biophysical methods (41–43). It should be noted that Rh molecules in native disk membranes are supposed to be in the paracrystalline state (44). However, due to moderate strength of interaction between Rh molecules, Rh oligomers and paracrystals are thought to be rather transient and dynamic entities (45,46). The interaction between Rh molecules would allow clustering of Rh only in an extraordinarily high concentration of Rh as in the disk membrane ($2.5 \times 10^4/\mu m^2$), whereas the concentration of Rh in this membrane is several orders smaller. Therefore, it would be reasonable to assume that the dimerization and higher-order organization of Rh molecules hardly occurred in this model system.

It was rather surprising that Rh had a high mobility, because it is generally assumed that integral membrane proteins are not mobile in a supported membrane (47). We confirmed the integration of Rh into the bilayer by the modulated diffusion coefficients in different lipid compositions. For example, Rh molecules diffused much faster in bilayers composed of DOPC (median diffusion coefficient: 1.44 $\mu m^2\ s^{-1}$ ($N = 57$)) than those composed of DOPC/DPPC/Chol. The diffusion coefficients of Rh were also modulated in different regions of a patterned bilayer (R_0 and R_1) (Fig. 6). Furthermore, activation of Rh altered the diffusion coefficients of G_t, strongly supporting the functional reconstitution of Rh. We reason that the observed mobility of Rh was due to its rather compact structure, which makes the protein mostly buried in the bilayer (48). We observed that the diffusion coefficients of Cy7- and Fab′-labeled Rh were identical. We assume that the orientation of Cy7-Rh in the bilayer was random, whereas Rh-Fab′ was mostly reconstituted with the C-terminus facing the bulk aqueous phase, because the Fab′ section cannot permeate through the bilayer membrane. Although the orientation of Rh molecules may affect the diffusion of Rh, partially due to their posttranslational glycosylation, these effects were not clearly observed in the obtained results.

We studied the localization and diffusion of Rh and G_t in R_0 and R_1, where L_o and L_d phases were enriched, respectively. The observed diffusion coefficients of Rh and G_t were significantly varied in R_0 and R_1. In the case of G_t, D was larger in R_0. The retarded diffusion of G_t in R_1 is presumably due to the obstruction by polymeric bilayer domains. We previously observed that polymeric bilayer domains have the average diameter of ~20 nm, and effectively obstructed the lateral diffusion of lipid molecules (24). On the other hand, D was larger in R_1 in the case of Rh. Although the diffusion coefficients of Rh and G_t in R_1 cannot be directly compared, because the obstruction depends on the density of polymeric domains, the slower diffusion of Rh in R_0 should be due to the obstruction by L_o domains. Because Rh is an integral membrane protein,

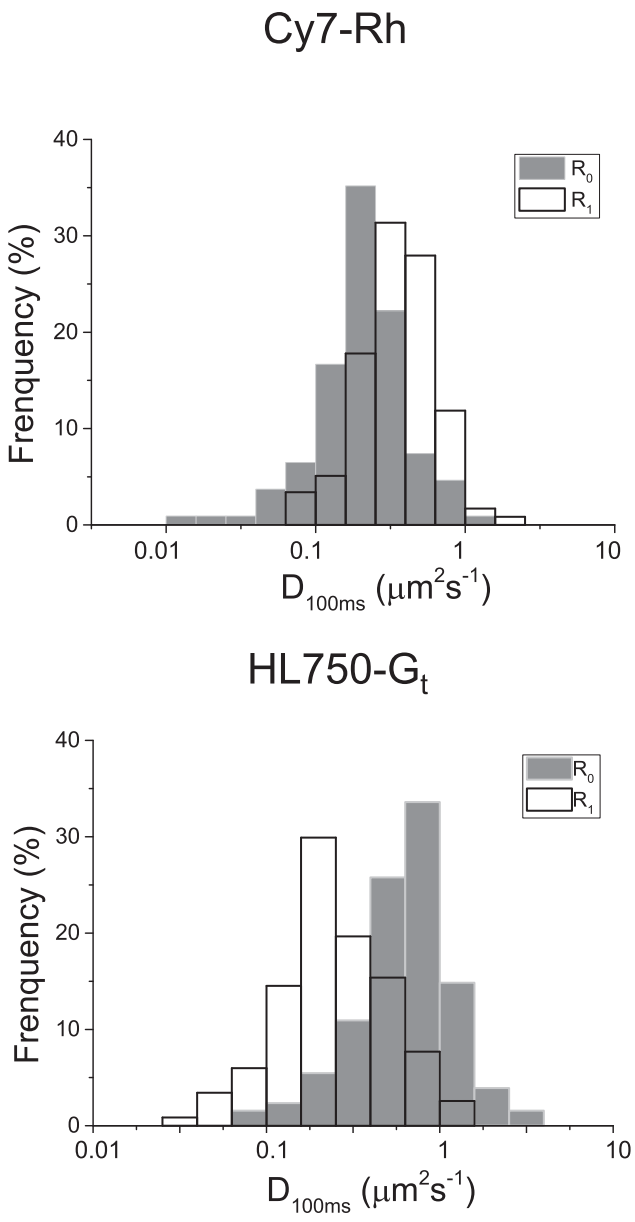

FIGURE 6 Diffusion coefficients of Rh and G_t in R_0 and R_1: The histograms of the diffusion coefficients obtained from the trajectories of Cy7-Rh and HL750-G_t in R_0 and R_1 (Cy7-Rh: $N = 108$ (R_0), $N = 118$ (R_1); and HL750-G_t: $N = 128$ (R_0), $N = 117$ (R_1)).

its diffusion is expected to be more strongly influenced by the lipid membrane environment (49,50). We observed that both Rh and G_t were predominantly localized in R_1, suggesting their preferential partitioning in L_d phase. We could evaluate the L_o/L_d partition coefficients of Rh and G_t by estimating the distribution of L_o and L_d phases using Rho-PE as a standard (38). From the obtained partition coefficients, it was concluded that Rh and G_t had a strong affinity toward L_d phase. It is consistent with the previous biochemical studies, which found that Rh and $G\alpha_t$ are mainly localized in the nonraft region before activation (11). As the biochemical results have demonstrated that G_t becomes highly raftophilic upon Rh* binding (11), it is desirable to be able to assess the distribution of Rh*-G_t complex in R_1 and R_0, though we have not yet succeeded to reconstitute enough amount of Rh*-G_t complex into SPB to evaluate its distribution. The amount of Rh molecules incorporated was rather limited due to the formation of immobile aggregates. It is an important technical challenge to realize a higher density of Rh for reconstructing dimer and paracrystals of Rh.

In the studies using model membranes, it is important to consider the potential artifacts and systematic discrepancies from the native membranes. An important question is if the presence of polymeric bilayer is affecting the partitioning of Rh and G_t. The results in Fig. S2 clearly demonstrated that the distribution of Rh in R_0 and R_1 regions was not affected by the polymeric bilayer in R_1. Furthermore, the partition coefficients of Rh and G_t between L_o and L_d phases were not influenced by the polymeric area fractions (p) (Fig. S3). These results corroborate the premise that polymeric bilayer domains do not strongly influence the partitioning behaviors of embedded proteins. On the other hand, the diffusion coefficients of Rh and G_t are retarded by polymeric bilayer domains, which may affect the localization and interaction of Rh and G_t. Therefore, it should be important to carefully control the amount of polymeric bilayer and assess its influences on the protein-lipid interactions. Another concern in the reconstitution of Rh is the influences of detergents on the membrane properties. For assessing the effects of OG, we compared the diffusion coefficients of Rh at two final OG concentrations (0.73 and 6 mM) and obtained identical diffusion coefficients (Fig. S4). These results strongly support our premise that the use of detergent in these conditions does not essentially affect the obtained results. More generally, however, we need to stay cautious about the possibility that protein partitioning in a model membrane may have systematic drifts from the native membrane due to the fact that interactions other than those between lipid molecules (e.g., protein-protein, glycan-glycan, etc.) are playing critical roles in the native membrane (51). Furthermore, the diverse lipid compositions in native membranes should modulate the phase behavior and partition of proteins in a complex manner (52,53). Therefore, addressing the question of systematic discrepancies between model and native membranes is important in future studies, which in turn should give further insights into the molecular mechanisms of raft-associated membrane functions.

In summary, we established a methodology to reconstitute Rh and G_t into a model membrane with micropatterned L_o and L_d phases for studying the localization and lateral mobility of the proteins. Evaluation of the partition between L_o and L_d phases is important for studying the influences of lipid rafts to the functions of Rh and G_t. Conventionally, enrichment in DRMs was used to evaluate the association of proteins with lipid rafts. Recently, a more

quantitative approach is being applied by microscopically observing GUVs or GPMVs. The micropatterned model membrane with a defined spatial distribution of L_o/L_d phases should provide fresh possibilities to gauge the association of proteins to lipid rafts. Although GUVs and GPMVs are structurally closer to the native cell membranes, patterned model membrane on the solid support should be advantageous in that they are amenable to integration and parallel analyses. Because raft-associated membrane functions are complex phenomena, involving diverse lipid-lipid, lipid-protein, and protein-protein interactions, an in vitro experimental platform that enables quantitative assays of these interactions in a systematic and high-throughput manner would be valuable for elucidating the roles lipid rafts in a wide range of cellular functions.

SUPPORTING MATERIAL

Four figures and four movies are available at http://www.biophysj.org/biophysj/supplemental/S0006-3495(15)01054-1.

AUTHOR CONTRIBUTIONS

F.H. and K.M. designed the research; F.H. and Y.T. prepared rhodopsin and transducin; Y.T. and K.O. conducted the experiments; Y.T. and F.H. analyzed the results; and Y.T., F.H., and K.M. wrote the article.

ACKNOWLEDGMENTS

We thank Dr. Shohei Maekawa (Graduate School of Science, Kobe University) for supporting us with his lab infrastructures. Discussion and helpful suggestions from Dr. Kenichi Suzuki and Dr. Rinsi Kasai (Kyoto University) are appreciated.

This work was supported by a Grant-in-Aid for Scientific research from Japan Society for the Promotion of Science (No. 26291031) and Hyogo Science and Technology Association.

REFERENCES

1. Simons, K., and D. Toomre. 2000. Lipid rafts and signal transduction. *Nat. Rev. Mol. Cell Biol.* 1:31–39.
2. Kusumi, A., I. Koyama-Honda, and K. Suzuki. 2004. Molecular dynamics and interactions for creation of stimulation-induced stabilized rafts from small unstable steady-state rafts. *Traffic.* 5:213–230.
3. Lingwood, D., and K. Simons. 2010. Lipid rafts as a membrane-organizing principle. *Science.* 327:46–50.
4. Oates, J., and A. Watts. 2011. Uncovering the intimate relationship between lipids, cholesterol and GPCR activation. *Curr. Opin. Struct. Biol.* 21:802–807.
5. Yang, J. P., T. Cirico, …, W. Kudlicki. 2011. Cell-free synthesis of a functional G protein-coupled receptor complexed with nanometer scale bilayer discs. *BMC Biotechnol.* 11:57.
6. Pike, L. J. 2003. Lipid rafts: bringing order to chaos. *J. Lipid Res.* 44:655–667.
7. Zheng, H., E. A. Pearsall, …, P. Y. Law. 2012. Palmitoylation and membrane cholesterol stabilize μ-opioid receptor homodimerization and G protein coupling. *BMC Cell Biol.* 13:6.
8. O'Brien, P. J., and M. Zatz. 1984. Acylation of bovine rhodopsin by ^{3}H palmitic acid. *J. Biol. Chem.* 259:5054–5057.
9. Fukada, Y., T. Takao, …, Y. Shimonishi. 1990. Farnesylated γ-subunit of photoreceptor G protein indispensable for GTP-binding. *Nature.* 346:658–660.
10. Kokame, K., Y. Fukada, …, Y. Shimonishi. 1992. Lipid modification at the N terminus of photoreceptor G-protein α-subunit. *Nature.* 359:749–752.
11. Seno, K., M. Kishimoto, …, F. Hayashi. 2001. Light- and guanosine 5′-3-O-(thio)triphosphate-sensitive localization of a G protein and its effector on detergent-resistant membrane rafts in rod photoreceptor outer segments. *J. Biol. Chem.* 276:20813–20816.
12. Alves, I. D., G. F. Salgado, …, V. J. Hruby. 2005. Phosphatidylethanolamine enhances rhodopsin photoactivation and transducin binding in a solid supported lipid bilayer as determined using plasmon-waveguide resonance spectroscopy. *Biophys. J.* 88:198–210.
13. Soubias, O., and K. Gawrisch. 2012. The role of the lipid matrix for structure and function of the GPCR rhodopsin. *Biochim. Biophys. Acta.* 1818:234–240.
14. Jacobson, K., O. G. Mouritsen, and R. G. Anderson. 2007. Lipid rafts: at a crossroad between cell biology and physics. *Nat. Cell Biol.* 9:7–14.
15. Macdonald, J. L., and L. J. Pike. 2005. A simplified method for the preparation of detergent-free lipid rafts. *J. Lipid Res.* 46:1061–1067.
16. Kahya, N., D. A. Brown, and P. Schwille. 2005. Raft partitioning and dynamic behavior of human placental alkaline phosphatase in giant unilamellar vesicles. *Biochemistry.* 44:7479–7489.
17. Baumgart, T., A. T. Hammond, …, W. W. Webb. 2007. Large-scale fluid/fluid phase separation of proteins and lipids in giant plasma membrane vesicles. *Proc. Natl. Acad. Sci. USA.* 104:3165–3170.
18. Gutierrez, M. G., and N. Malmstadt. 2014. Human serotonin receptor 5-HT(1A) preferentially segregates to the liquid disordered phase in synthetic lipid bilayers. *J. Am. Chem. Soc.* 136:13530–13533.
19. Ge, Y., A. P. Siegel, …, C. A. Naumann. 2014. Ligand binding alters dimerization and sequestering of urokinase receptors in raft-mimicking lipid mixtures. *Biophys. J.* 107:2101–2111.
20. Siegel, A. P., A. Kimble-Hill, …, C. A. Naumann. 2011. Native ligands change integrin sequestering but not oligomerization in raft-mimicking lipid mixtures. *Biophys. J.* 101:1642–1650.
21. Yoon, T. Y., C. Jeong, …, S. D. Lee. 2006. Topographic control of lipid-raft reconstitution in model membranes. *Nat. Mater.* 5:281–285.
22. Roder, F., O. Birkholz, …, J. Piehler. 2013. Spatial organization of lipid phases in micropatterned polymer-supported membranes. *J. Am. Chem. Soc.* 135:1189–1192.
23. Okazaki, T., Y. Tatsu, and K. Morigaki. 2010. Phase separation of lipid microdomains controlled by polymerized lipid bilayer matrices. *Langmuir.* 26:4126–4129.
24. Okazaki, T., T. Inaba, …, K. Morigaki. 2009. Polymerized lipid bilayers on a solid substrate: morphologies and obstruction of lateral diffusion. *Langmuir.* 25:345–351.
25. Okada, F., and K. Morigaki. 2015. Micropatterned model membrane with quantitatively controlled separation of lipid phases. *RSC Advances.* 5:1507–1513.
26. Heyse, S., O. P. Ernst, …, H. Vogel. 1998. Incorporation of rhodopsin in laterally structured supported membranes: observation of transducin activation with spatially and time-resolved surface plasmon resonance. *Biochemistry.* 37:507–522.
27. Subramaniam, V., I. D. Alves, …, S. S. Saavedra. 2005. Rhodopsin reconstituted into a planar-supported lipid bilayer retains photoactivity after cross-linking polymerization of lipid monomers. *J. Am. Chem. Soc.* 127:5320–5321.
28. Hayashi, F., and A. Yamazaki. 1991. Polymorphism in purified guanylate cyclase from vertebrate rod photoreceptors. *Proc. Natl. Acad. Sci. USA.* 88:4746–4750.
29. Litman, B. J. 1982. Purification of rhodopsin by concanavalin A affinity chromatography. *Methods Enzymol.* 81:150–153.

30. Yamazaki, A., M. Tatsumi, …, M. W. Bitensky. 1987. The GTP-binding protein of rod outer segments. I. Role of each subunit in the GTP hydrolytic cycle. *J. Biol. Chem.* 262:9316–9323.

31. Wald, G., and P. K. Brown. 1953. The molar extinction of rhodopsin. *J. Gen. Physiol.* 37:189–200.

32. MacKenzie, D., A. Arendt, …, R. S. Molday. 1984. Localization of binding sites for carboxyl terminal specific anti-rhodopsin monoclonal antibodies using synthetic peptides. *Biochemistry.* 23:6544–6549.

33. Ichinose, J., M. Murata, …, Y. Sako. 2004. EGF signalling amplification induced by dynamic clustering of EGFR. *Biochem. Biophys. Res. Commun.* 324:1143–1149.

34. Yamazaki, A., M. Tatsumi, and M. W. Bitensky. 1988. Purification of rod outer segment GTP-binding protein subunits and cGMP phosphodiesterase by single-step column chromatography. *Methods Enzymol.* 159:702–710.

35. Morigaki, K., H. Schönherr, and T. Okazaki. 2007. Polymerization of diacetylene phospholipid bilayers on solid substrate: influence of the film deposition temperature. *Langmuir.* 23:12254–12260.

36. Tarantino, N., J. Y. Tinevez, …, E. Laplantine. 2014. TNF and IL-1 exhibit distinct ubiquitin requirements for inducing NEMO-IKK supramolecular structures. *J. Cell Biol.* 204:231–245.

37. Saxton, M. J., and K. Jacobson. 1997. Single-particle tracking: applications to membrane dynamics. *Annu. Rev. Biophys. Biomol. Struct.* 26:373–399.

38. Chiantia, S., J. Ries, …, P. Schwille. 2006. Combined AFM and two-focus SFCS study of raft-exhibiting model membranes. *ChemPhysChem.* 7:2409–2418.

39. Kameyama, K., and T. Takagi. 1990. Micellar properties of octylglucoside in aqueous solutions. *J. Colloid Interface Sci.* 137:1–10.

40. Kühn, H. 1980. Light- and GTP-regulated interaction of GTPase and other proteins with bovine photoreceptor membranes. *Nature.* 283:587–589.

41. Liebman, P. A., and G. Entine. 1974. Lateral diffusion of visual pigment in photoreceptor disk membranes. *Science.* 185:457–459.

42. Poo, M., and R. A. Cone. 1974. Lateral diffusion of rhodopsin in the photoreceptor membrane. *Nature.* 247:438–441.

43. Wang, Q., X. Zhang, …, T. G. Wensel. 2008. Activation-dependent hindrance of photoreceptor G protein diffusion by lipid microdomains. *J. Biol. Chem.* 283:30015–30024.

44. Fotiadis, D., Y. Liang, …, K. Palczewski. 2003. Atomic-force microscopy: rhodopsin dimers in native disc membranes. *Nature.* 421:127–128.

45. Comar, W. D., S. M. Schubert, …, A. W. Smith. 2014. Time-resolved fluorescence spectroscopy measures clustering and mobility of a G protein-coupled receptor opsin in live cell membranes. *J. Am. Chem. Soc.* 136:8342–8349.

46. Whited, A. M., and P. S. Park. 2015. Nanodomain organization of rhodopsin in native human and murine rod outer segment disc membranes. *Biochim. Biophys. Acta.* 1848 (1 Pt A):26–34.

47. Sumino, A., T. Dewa, …, M. Nango. 2011. Construction and structural analysis of tethered lipid bilayer containing photosynthetic antenna proteins for functional analysis. *Biomacromolecules.* 12:2850–2858.

48. Palczewski, K., T. Kumasaka, …, M. Miyano. 2000. Crystal structure of rhodopsin: a G protein-coupled receptor. *Science.* 289:739–745.

49. Vaz, L. C. W., F. Goodsaid-Zalduonodo, and K. Jacobson. 1984. Lateral diffusion of lipids and proteins in bilayer membranes. *FEBS Lett.* 174:199–207.

50. Quemeneur, F., J. K. Sigurdsson, …, D. Lacoste. 2014. Shape matters in protein mobility within membranes. *Proc. Natl. Acad. Sci. USA.* 111:5083–5087.

51. Kaiser, H. J., D. Lingwood, …, K. Simons. 2009. Order of lipid phases in model and plasma membranes. *Proc. Natl. Acad. Sci. USA.* 106:16645–16650.

52. Shogomori, H., A. T. Hammond, …, D. A. Brown. 2005. Palmitoylation and intracellular domain interactions both contribute to raft targeting of linker for activation of T cells. *J. Biol. Chem.* 280:18931–18942.

53. Sezgin, E., T. Gutmann, …, P. Schwille. 2015. Adaptive lipid packing and bioactivity in membrane domains. *PLoS One.* 10:e0123930.